Polylactide-Recycled Wood Fiber Composites

Srikanth Pilla,[1] Shaoqin Gong,[1,2] Eric O'Neill,[3] Liqiang Yang,[1] Roger M. Rowell[3]

[1]*Department of Mechanical Engineering, University of Wisconsin-Milwaukee, Wisconsin*
[2]*Department of Materials, University of Wisconsin-Milwaukee, Wisconsin*
[3]*Forest Products Laboratory, United States Department of Agriculture, Madison, Wisconsin*

Received 10 October 2007; accepted 9 June 2008
DOI 10.1002/app.28860
Published online 26 September 2008 in Wiley InterScience (www.interscience.wiley.com).

ABSTRACT: Polylactide (PLA)-recycled wood fiber (RWF) composites with a small amount of silane were compounded using a kinetic-mixer and molded using an injection molding machine. The molded PLA-RWF composites were characterized using gel permeation chromatography, scanning electron microscope, X-ray diffraction, differential scanning calorimeter, tensile testing machine, and a dynamic mechanical analyzer. As observed in the stress–strain plots, the amount of necking before fracture decreased with an increasing RWF content. Similarly, the strain-at-break also decreased with the RWF content. The tensile strength remained the same irrespective of the RWF content. Both the tensile modulus and the storage modulus of the PLA-RWF composites increased with the RWF content. The degree of crystallinity of the PLA increased with the addition of RWF. No reduction in the number–average molecular weight (M_n) was observed for pure PLA and PLA-10%RWF-0.5%Silane composites after injection molding; however, substantial reduction in M_n was found in PLA-20%RWF-0.5%Silane composites. Finally, a theoretical model based on Halpin–Tsai empirical relations is presented to compare the theoretical results with that of the experimental results. © 2008 Wiley Periodicals, Inc. J Appl Polym Sci 111: 37–47, 2009

Key words: polylactide; silane; recycled wood fiber; composite; biobased; Halpin–Tsai; crystallization; molecular weight

INTRODUCTION

Biobased polymers such as polylactide (PLA) have drawn much attention in recent years because of their biodegradable nature.[1–3] Biobased polymers can reduce global dependency on fossil fuels and are more CO_2 neutral. PLA is an aliphatic polyester prepared either by direct condensation of lactic acid or by ring-opening polymerization of lactide, the cyclic-dimer of lactic acid (α-hydroxy acid).[4] PLA has high modulus, reasonable strength, excellent flavor and aroma barrier properties, and good heat sealability[5]; however, widespread application of PLA is limited because of its high cost and certain inferior material properties such as a low heat deflection temperature.[6–9] Thus, to increase the usability of PLA, the material cost must be reduced while maintaining and/or improving the material properties.

Various types of fillers, such as talc, calcium carbonate, mica, glass, and carbon fibers, can be used in a polymer matrix to decrease its cost and improve its material properties.[10] However, owing to growing environmental concerns, researchers are shifting their focus toward cellulose-based fillers such as wood fibers.[11] Cellulose fibers have several advantages over traditional fillers such as biodegradability, renewable nature, low cost, low density, low energy consumption, high specific strength and stiffness, CO_2 sequestration, and less wear on machinery.[11,12] Despite these advantages, cellulose-based wood fibers have not been used extensively as reinforcements in polymers because of their low bulk density, low thermal stability, poor dispersion in the polymer melt, and tendency to absorb moisture.[13,14]

This study focuses on recycled wood fibers (RWFs). When RWFs are blended with biobased and biodegradable polymer such as PLA, a fully biobased and biodegradable composite with enhanced material properties is formed. Thus, the use of RWFs in the production of plastics will reduce the amount of solid waste generated, improve the value of RWFs, and reduce the overall cost of the plastic composites.[15] Many automakers are interested in such plastics because of the intense competition to manufacture ecofriendly vehicles.[16]

Although cellulose-based wood fibers can potentially provide enhanced properties to the polymer matrix, a major limitation in their use as fillers in polymers is the poor interfacial adhesion.[17] Thus, it is important to use a coupling agent to provide better adhesion. Xue et al.[18] demonstrated how the

Correspondence to: S. Gong (sgong@uwm.edu).
Contract grant sponsor: National Science Foundation; contract grant number: CMMI-0544729.

addition of maleic anhydride increased the compatibility of polypropylene and aspen wood fiber. Pilla et al.[3] have investigated PLA-pine wood flour composites with and without silane and found that silane-treated composites enhanced mechanical properties compared with the untreated composites. Colom et al.[19] have used both silane and maleated ethylene as coupling agents in polyethylene-aspen fiber composites and found that silane-treated composites have better mechanical properties than composites treated with maleated ethylene. Thus, silane was used in this study as the coupling agent between PLA and RWF.

This article reports the investigation of a new bio-based, ecofriendly PLA-RWF composite. Various properties were studied, including mechanical (static and dynamic) and thermal properties. A theoretical model to predict the Young's modulus of the composite system also is presented.

EXPERIMENTAL SECTION

Materials

Polylactide (NatureWorks™ PLA 3001D) in pellet form was obtained from NatureWorks® LLC, Minnetonka, MN. It has a specific gravity of 1.24 and a melt flow index around 15 g/10 min (190°C/2.16 Kg). PLA 3001D was synthesized from ~ 92% L-lactide and 8% meso-lactide.[20] The fibers used in this study are commercially available RWFs obtained from the GP Lionite Plant in Phillips, WI. The fibers consist of a blend of hardwood and softwood namely aspen, oak, pine, basswood, etc. GE Silicones—Silquest A-174® silane (gamma-methacryloxypropyltrimethoxysilane), obtained from Witco Corp., was used as the coupling agent. The chemical formula for silane is given below:

$$CH_2{=}C(CH_3)CO_2CH_2CH_2CH_2Si(OCH_3)_3$$

Methods

Processing PLA with RWF

Prior to processing, both PLA and RWF were dried in an oven at 55 and 105°C, respectively, for about 4 h to remove any moisture that had absorbed during storage. A kinetic mixer (K-mixer) (Vanzetti Systems Series 3009) blended the PLA and RWF. First, the RWF was fed into the K-mixer and a few drops of silane (0.5% of RWF content) were added. The K-mixer was turned on and once it reached 5000 rpm (revolutions per minute), it was turned off. This helped to disperse the silane within the RWF. The silane percentage (0.5%) employed in this study is a percentage relative to the RWF content in the formulation; thus, the higher the RWF content, the higher the silane content will be. Subsequently, the PLA pellets (weighed for appropriate proportion) were added to the mixing chamber and the machine was turned on again to raise the rpm to 5000. Heat generated from the frictional force caused the PLA pellets to melt.

As the temperature increased to a preset value (204°C), the chamber door was opened and the molten blend of PLA and RWF was placed into the basket located below the chamber. The molten blend was cooled in a cold press, granulated, and dried at 55°C for 1 h. The dry material (granulated) was then fed into the hopper of the injection molding machine (Cincinnati Milacron 33-ton). Three samples were prepared (PLA, PLA-10%RWF-0.5%Silane, and PLA-20%RWF-0.5%Silane). As the volume of the K-mixer chamber is limited, PLA-RWF composites with a higher RWF content (>20%) became too difficult to process because the volume of the RWF became too large as a result of its very low bulk density.

During the injection molding process, the following temperatures were set at respective zones: 202°C near the feeder, 204°C in the middle zone(s), and 207°C at the injection tip. A variable pack/hold pressure of 4.83–6.89 MPa was used depending on the weight percentage of the RWF (4.83 MPa for 10% and up to 6.89 MPa for 20%). A pack/hold time of 15 s also was used to ensure maximum material in the mold. Because PLA has a low glass transition temperature (T_g), a mold temperature of 19°C was maintained to allow adequate freezing in the allotted cooling time. A cooling time of 40 s per part was provided to ensure the part did not break upon die separation.

Gel permeation chromatography

The number–average molecular weight (M_n) and polydispersity index (PDI) of PLA presented in all three types of samples (pure PLA, PLA-10%RWF-0.5%Silane, and PLA-20%RWF-0.5%Silane composites), after the injection molding process as well as that of the pure PLA pellets as received from the supplier, were determined by gel permeation chromatography (GPC) on a Viscotek HPLC system equipped with a model VE3580 refractive-index detector and an I-MBHMW-3078/I-MBLMW-3078 column set. Chloroform was used as an eluent (flow rate 1.0 mL/min) at 35°C. The PLA samples were prepared as 1.0% wt/vol solutions in chloroform, with ~ 10 μL of sample injected into GPC. Prior to this injection, the dissolved solution was filtered using a 0.2-μm PTFE filter. For the PLA-RWF samples, the filtration process was done in two stages: (1) using a standard filter paper and (2) using the

PTFE filter. The M_n was calibrated by polystyrene standards.

Scanning electron microscopy

The fracture surfaces from the tensile tests were examined using SEM (Hitachi *S*-570) operated at 10 kV. All specimens were sputter-coated with a thin layer of gold (20 nm) prior to examination.

Wide-angle X-ray diffraction

WAXRD analysis was performed on Scintag XDS 2000 with Ni-filtered Cu Ka radiation (1.5418 A°) at room temperature in the range of $2\theta = 5$–40° with a scanning rate of 1°/min.

Differential scanning calorimetry

Thermal analysis of injection-molded specimens was carried out using DSC (TA Instruments, Auto DSC-Q20). The sample used for testing was sliced from the injection-molded specimen. Two different experiments were conducted. In the first experiment (referred to as DSC experiment-1), the sample was first heated from 40 to 180°C, kept isothermal for 3 min, cooled to 0°C, and then reheated to 200°C with a heating and cooling rate of 10°C/min. In the second experiment (referred to as DSC experiment-2), the sample was first heated from 40 to 180°C, kept isothermal for 3 min, quenched in liquid N_2, and then reheated to 200°C. The heating rate was 10°C/min. The DSC experiment-2 was conducted to simulate the rapid cooling process experienced by the injection-molded samples during the injection molding process.

Tensile testing

The static tensile properties (modulus, strength, toughness, elongation-at-break) were measured at room temperature (25°C) and atmospheric conditions (relative humidity of $\sim 50\% \pm 5\%$) with a 5 kN load cell on an Instron Model 5566 tensile tester. The cross-head speed was set at 5 mm/min. The extensometer used was an MTS 634.31E-24 with a 1-in. gauge length. All tests were carried out according to the ASTM standard (ASTM-D638). Five specimens of each sample were tested and the average results were reported. All samples were tested after being subjected to room temperature and atmospheric conditions for $\sim$ 2 weeks.

Dynamic mechanical analysis

The dynamic mechanical spectra of the different specimens, cut from injection-molded samples, were obtained using a dynamic mechanical analyzer (TA instrument, model DMA Q800). Rectangular specimens ($\sim$ 17.7 mm $\times$ 12.8 mm $\times$ 3.1 mm, respectively, for $L \times B \times H$) were tested in a single-cantilever mode. They were heated at a rate of 3°C/min from 0 to 85°C with a frequency of 1 Hz and strain of 0.02%, which is in the linear viscoelastic region as determined by a strain sweep.

TABLE I
The M_n and PDI of the PLA in PLA Pellets as Received and the Three Samples Subjected to the Injection Molding Process: pure PLA, PLA-10%RWF-0.5%Silane, and PLA-20%RWF-0.5%Silane, were determined by GPC

Sample	M_n	PDI
PLA pellets	61,257	2.2
PLA (processed)	61,710	2.3
PLA-10%RWF-0.5%Silane	61,265	2.1
PLA-20%RWF-0.5%Silane	43,005	2.1

RESULTS AND DISCUSSION

Molecular weight measurement

The M_n and PDI values of all four samples measured using GPC are tabulated in Table I. As can be observed from the table, the M_n of PLA did not vary much among the first three samples, indicating that no PLA degradation occurred as a result of the injection molding process in the pure PLA and PLA-10%RWF-0.5%Silane composite. However, the M_n of PLA in the PLA-20%RWF-0.5%Silane composite was reduced by $\sim$ 29%. It is likely that there was a small amount of residual moisture in the RWF that triggered the PLA molecular degradation through hydrolysis at the high processing temperature.

Morphology of the RWF, PLA, and PLA-RWF composites

As shown in Figure 1, RWF has a ribbon-like structure with a width of several tens of microns. The length of the fiber is $\sim$ 1–3 mm.[21] Unlike pine wood flour, which has a rough surface,[3] the surface of the RWF is smooth; thus, it is difficult to achieve good interfacial adhesion via the mechanical interlocking between RWF and PLA. The fracture surface of the fractured tensile specimens resulting from the tensile test was used to study the morphology of the PLA and PLA-RWF composites using SEM. Figures 2–4 show the representative images of the pure PLA, PLA-10%RWF-0.5%Silane, and PLA-20%RWF-0.5% Silane, respectively. The RWFs are uniformly dispersed within the PLA matrix in both PLA-RWF composites. Fibers protruding out of the surface as

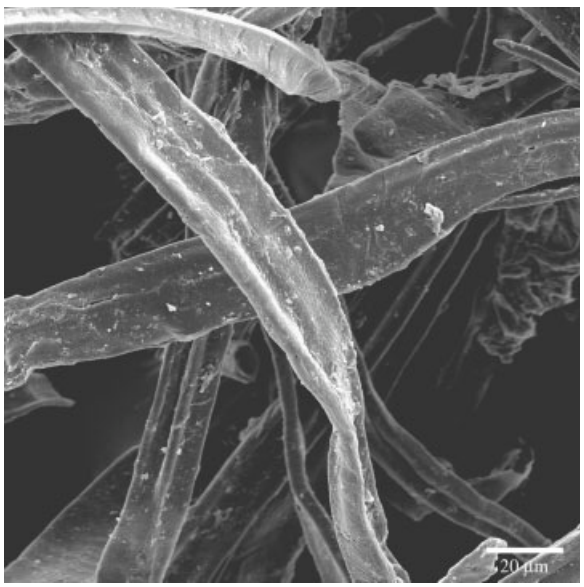

Figure 1 SEM image of the RWF-20 μm.

well as holes resulting from the fiber pull-out can be observed on the fracture surfaces of the two composite samples, as shown in Figures 3(b) and 4(b). This phenomenon indicates that the interfacial strength between the RWF and the PLA is generally lower than the strength of the RWF itself, despite the addition of silane to improve the interfacial adhesion between the RWF and PLA. The increment in RWF content is highly visible in Figure 4 compared with Figure 3. Thus, the stiffness of the 20%RWF sample should be higher than the 10%RWF,[22] which is confirmed in the next section of this article. All three samples had a smooth fracture surface, indicating the lack of significant plastic deformation.

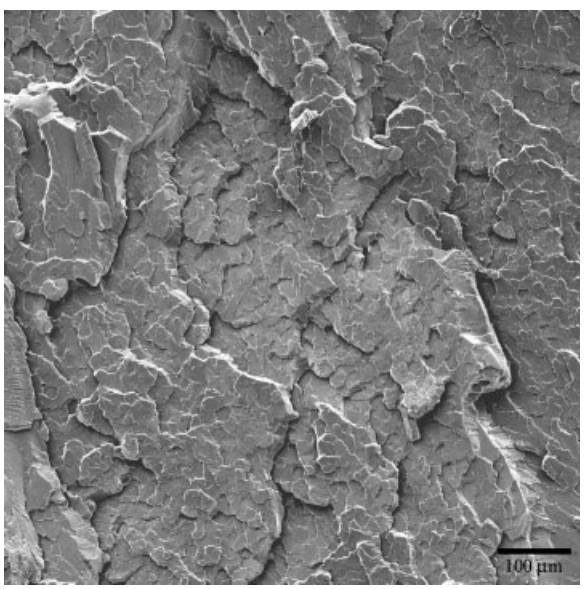

Figure 2 SEM image of pure PLA-100 μm.

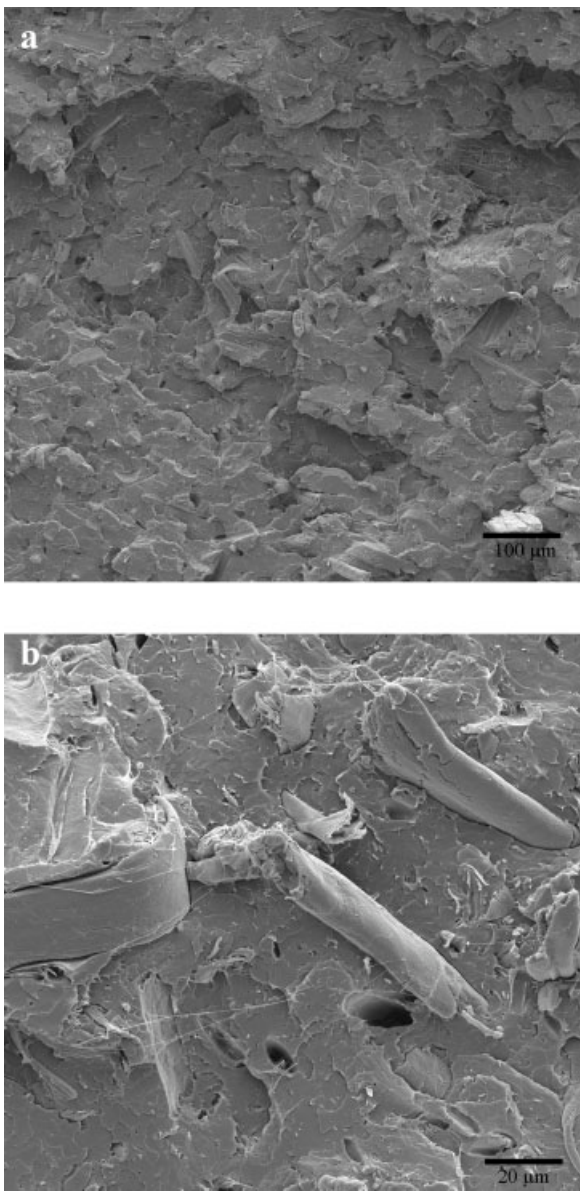

Figure 3 SEM images of the PLA-10%RWF-0.5%Silane composite—(a) 100 μm; (b) 20 μm.

WAXRD analysis

Pure PLA, RWF, and PLA-RWF composites were characterized by WAXRD to study the effect of RWF and its loading level on the crystalline structure of PLA. The XRD patterns of all the materials are shown in Figure 5, in which pure PLA exhibited a broad amorphous peak with the 2θ value ranging from 10.62 to 25.16°. However, a sharp peak was observed at $2\theta = 16.4°$ resulting from the crystalline structure present in the PLA samples; thus, PLA can be considered as a semicrystalline polymer. This agrees with studies conducted by Mathew et al.[23] The XRD pattern of RWF shows a sharp peak at $2\theta = 22.74°$ and a broad peak around the region $2\theta = 14–17°$. According to the Bragg's diffraction equation,[24] the *d* (interplanar spacing) values, for the

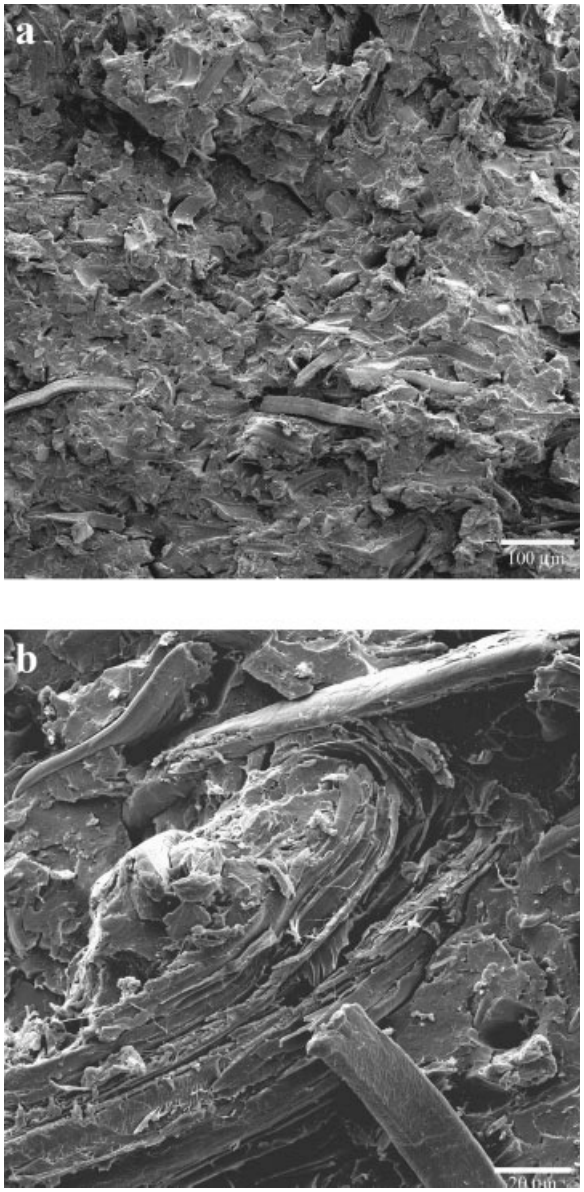

Figure 4 SEM images of the PLA-20%RWF-0.5%Silane composite—(a) 100 μm; (b) 20 μm.

first-order diffraction, associated with $2\theta = 16.4$ and 22.74° are 5.39 and 3.91 Å, respectively. Both PLA-RWF composites, i.e., PLA-10%RWF-0.5%Silane and PLA-20%RWF-0.5%Silane exhibited peaks at $2\theta = 16.5°$ and 22.3°, corresponding with the crystalline structure of PLA and RWF, respectively. A quantitative analysis of the degree of crystallinity as measured using DSC is provided in the next section.

Differential scanning calorimetry

DSC was used to study the crystallization behavior of the PLA and PLA-RWF composites. Two types of DSC experiments were conducted: DSC experiment-1 and DSC experiment-2. For DSC experiment-1, a ramp rate of 10°C/min was used for all the three cycles, i.e., heating, cooling and heating; for DSC experiment-2, the same ramp rate was maintained for both the heating cycles but quench cooling was employed in between the heating cycles. The thermograms obtained from the first and second heating cycles of the DSC experiment-1 are shown in Figures 6(a) and 6(b),

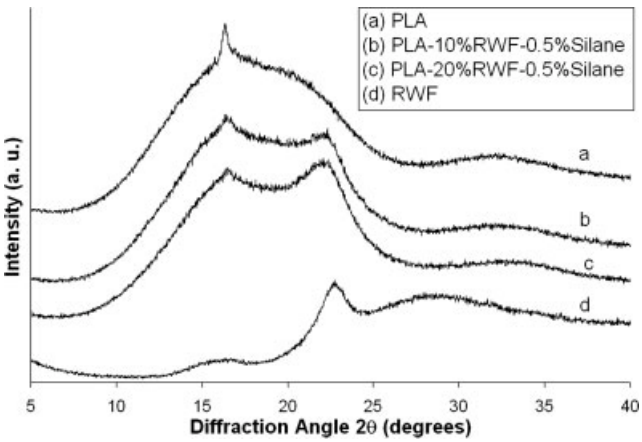

Figure 5 WAXRD patterns of pure PLA, RWF, and PLA-RWF composites.

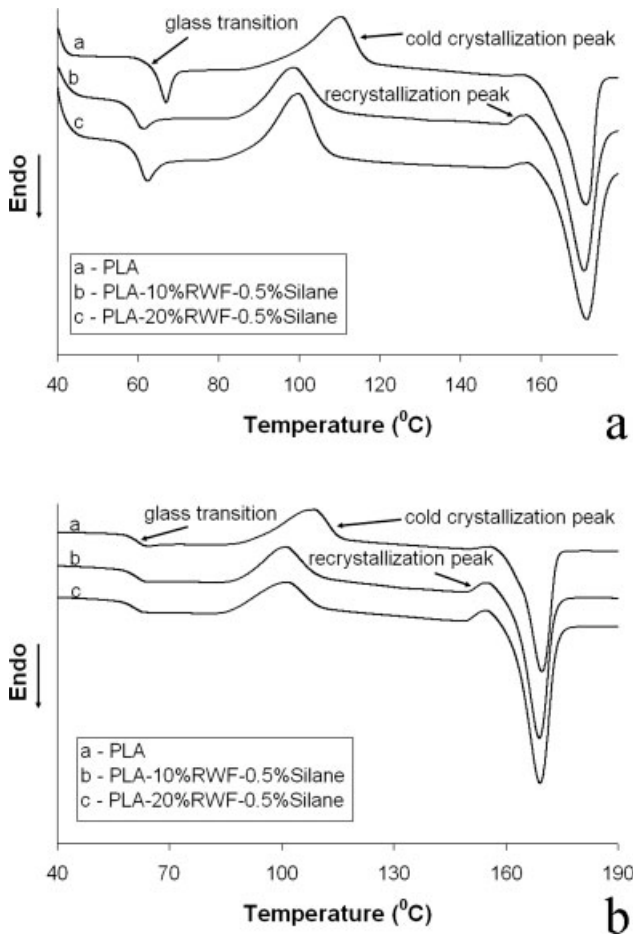

Figure 6 Melting curves of the PLA and PLA-RWF composites; data obtained from the DSC experiment-1: (a) first heating cycle and (b) second heating cycle.

TABLE II
Thermal Characteristics of the PLA and PLA-RWF Composites

Sample	T_{cc} (°C)	ΔH_c (J/g)	T_r (°C)	ΔH_r (J/g)	T_m (°C)	ΔH_m (J/g)	χ_c (%)
A. First heating cycle (DSC experiment-1)							
PLA	110.5	−27.2	–	–	171.1	36.9	10
PLA-10%RWF-0.5%Silane	98.8	−20.9	156.3	−1.4	170.7	35.8	16
PLA-20%RWF-0.5%Silane	99.8	−21.1	156.7	−0.7	171.3	34.1	17
B. Second heating cycle (DSC experiment-1: 10°C cooling rate)							
PLA	108.7	−24.8	155.9	−0.5	169.7	36.8	12
PLA-10%RWF-0.5%Silane	101.5	−18.8	155.3	−1.9	169.1	37.3	20
PLA-20%RWF-0.5%Silane	101.8	−16.1	154.9	−1.8	169.2	37.3	26
C. First heating cycle (DSC experiment-2)							
PLA	109.3	−28.9	–	–	172.7	38.6	10
PLA-10%RWF-0.5%Silane	98.7	−21.3	156.3	−1.6	170.2	35.4	15
PLA-20%RWF-0.5%Silane	97.8	−22.7	155.3	−0.9	169.9	35.6	16
D. Second heating cycle (DSC experiment-2: quench cooling)							
PLA	112.1	−32.8	–	–	170.9	40.0	8
PLA-10%RWF-0.5%Silane	100.4	−23.6	155.2	−1.1	168.9	37.5	15
PLA-20%RWF-0.5%Silane	99.7	−21.3	154.4	−1.2	168.3	33.5	15

T_{cc}, cold crystallization temperature; ΔH_c, cold crystallization enthalpy; T_r, recrystallization temperature; ΔH_r, recrystallization enthalpy; T_m, melting temperature; ΔH_m, melting enthalpy; χ_c, degree of crystallinity.

respectively. Table II presents the numerical values of the temperature and enthalpy obtained from the first and second heating cycles and the degree of crystallinity calculated from both the heating cycles. The data obtained from the first heating cycle provides information on the injection-molded samples, whereas the data obtained from the second heating cycle allows for a direct comparison of the crystallization behavior of different materials after erasing any previous thermal history through the first heating cycle.

The crystallinity of PLA is computed using the following equation[25]:

$$\chi_c(\%\ \text{Crystallinity}) = \frac{\Delta H_m}{\Delta H_m^0} \times \frac{100}{w} \tag{1}$$

where,

$\Delta H_m^0 - 93.7 \quad \text{J/g}$
$w -$ weight fraction of PLA in the sample

ΔH_m is the enthalpy for melting, ΔH_m^0 is the enthalpy of melting for a 100% crystalline PLA sample,[25] and w is the weight fraction of PLA in the sample. To determine the crystallinity of the sample, the extra heat absorbed by the crystallites formed during heating (i.e., cold crystallization) had to be subtracted from the total endothermic heat flow because of the melting of the whole crystallites.[26] Thus, the modified equation can be written as follows:

$$\chi_c(\%\ \text{Crystallinity}) = \frac{\Delta H_m - \Delta H_{cc}}{\Delta H_m^0} \times \frac{100}{w} \tag{2}$$

where,

ΔH_{cc} : Cold − Crystallization Enthalpy.

The DSC experiment-1

The thermograms of PLA and PLA-RWF composites obtained from the first heating are shown in Figure 6(a), in which an endotherm peak (in all the three specimens) exists near the glass transition phase because of physical aging of the polymeric materials.[27–29] This phenomenon is related to the inherent distribution of the relaxation times of polymer chains.[30] It also can be observed that two crystallization peaks exist for the composite specimens. The first peak, termed the cold crystallization peak, was at ~ 99 and 100°C for PLA-10%RWF-0.5%Silane and PLA-20%RWF-0.5%Silane specimens, respectively; the second peak, termed the recrystallization peak, occurred just before the melting peak at ~ 156 and 157°C, respectively, for PLA-10%RWF-0.5%Silane and PLA-20%RWF-0.5%Silane; however, no obvious recrystallization peak was observed for the pure PLA specimen. The recrystallization peaks observed in the composite specimens might be due to the restructuring of certain existing crystalline structures at higher temperatures.

The addition of RWF enhanced the crystallinity of PLA (Table II) because RWFs can act as nucleating agents during the crystallization process. This agrees with the findings from the literature that the addition of fillers enhances the crystallinity of PLA[3,31,32];

however, this increment in PLA crystallinity because of the addition of RWF was found to be the same for both composites, i.e., PLA-10%RWF-0.5%Silane and PLA-20%RWF-0.5%Silane. Finally, the cold crystallization peak of PLA was shifted to lower temperatures with the addition of RWFs. This agrees with the findings from the literature[33] that the presence of fillers can promote the initial cold crystallization of PLA matrix.

Figure 6(b) and Table II show the thermogram and numerically analyzed data of PLA and its composites, respectively, from the second heating cycle. Unlike the first heating cycle, the endotherm peaks near the T_g were not observed here because the enthalpic recovery that occurred during the first heating cycle is kinetic in nature. In addition, both a cold crystallization peak and a recrystallization peak were observed for all three types of specimens. The cold crystallization peak was observed at 108.7, 101.5, and 101.8°C for PLA, PLA-10%RWF-0.5%Silane, and PLA-20%RWF-0.5%Silane, respectively. Thus, the cold crystallization peak (T_{cc}) shifted to lower temperatures with the addition of RWFs. As stated earlier, this agrees with the findings from the literature[33] that the presence of fillers can promote the initial cold crystallization of PLA matrix. The recrystallization peak was observed at $\sim$ 155°C for all the three specimens.

Similar to the first heating cycle, the addition of RWF enhanced the crystallinity of PLA because RWF acted as nucleating agents. Additionally, the crystallinity increased with the RWF content. As shown in Table II, the degree of crystallinity for PLA-10%RWF-0.5%Silane and PLA-20%RWF-0.5%Silane was 20 and 26%, respectively. The relatively higher increment in crystallinity with the addition of RWF observed during the second heating cycle compared with the first heating cycle is likely due to much lower DSC cooling rate (10°C/min) experienced by the samples in the former compared with the much higher cooling rate (close to 200°C/min) experienced by the injection-molded samples in the latter. This topic is discussed in the next section; however, we can conclude that the addition of RWF increased the crystallinity by acting as a nucleating agent.

The DSC experiment-2

Because a difference was observed in the crystallinity of PLA and PLA-RWF composites measured during the first and second heating cycles in the DSC experiment-1, the DSC experiment-2 was conducted to simulate the faster cooling rate experienced during the injection molding process using the "quench" cooling process.

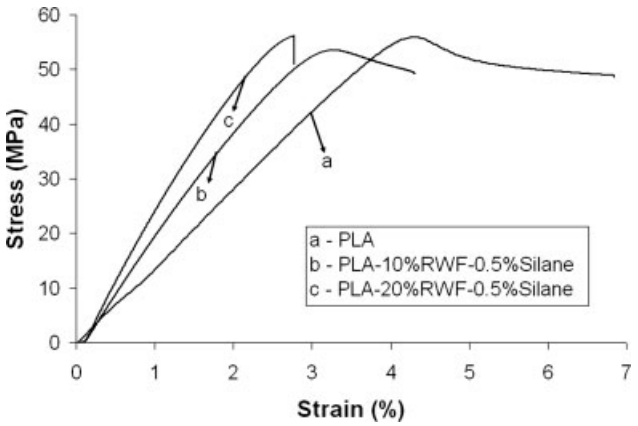

Figure 7 Tensile stress–strain curves of the PLA and PLA-RWF composites.

Table II shows the numerical values of temperatures and enthalpies of the two heating cycles of DSC experiment-2 along with the computed degree of crystallinity. It can be observed that the crystallinity obtained from the first and second heating cycle remained the same, which illustrates that by simulating the injection molding cooling rate, the crystallinity measured during both heating cycles can be matched.

Static mechanical properties

The static mechanical properties of PLA and PLA-RWF composites were measured via tensile testing. A representative stress–strain plot for each of the three types of specimens (PLA, PLA-10%RWF-0.5%Silane, and PLA-20%RWF-0.5%Silane) is presented in Figure 7, which shows that PLA and PLA-10%RWF-0.5%Silane exhibited necking before fracture, but such a phenomenon could not be observed in the PLA-20%RWF-0.5%Silane sample. In addition, the degree of necking observed in the pure PLA is much higher than that of the PLA-10%RWF-0.5%Silane sample. Necking is a mode of ductile flow of a material in tension; thus, adding more RWF reduced plastic deformation in the PLA-RWF composites and led to a more brittle fracture mode.

Toughness, which is the energy-to-fracture per-unit volume of the specimen,[34] is obtained by integrating the area under the stress–strain curve. As shown in the Table III, PLA has the highest toughness value of 5.5×10^6 J/m^3, followed by 1.5×10^6 J/m^3 for PLA-10%RWF-0.5%Silane, and 0.9×10^6 J/m^3 for PLA-20%RWF-0.5%Silane. Thus, the toughness of PLA decreased significantly with the addition of RWF. This could be attributed due to the fact that (1) RWF particles may act as stress concentrators in the composites and (2) RWF particles are rigid and brittle.[35] Similar to the observed trend with toughness, the strain-at-break (%) of PLA also

TABLE III
Mechanical Properties of PLA-Recycled Wood Fiber Composites

Sample	Fracture toughness (J/m^3)	Strain-at-break (%)	Young's modulus (MPa)	Ultimate tensile strength (MPa)
PLA	$5.5 \times 10^6 \pm 1.0 \times 10^6$	6.8 ± 0.1	638.9 ± 9.9	55.5 ± 0.6
PLA-10%RWF-0.5%Silane	$1.5 \times 10^6 \pm 0.1 \times 10^6$	4.3 ± 0.1	2032.7 ± 160.1	53.2 ± 0.9
PLA-20%RWF-0.5%Silane	$0.9 \times 10^6 \pm 0.1 \times 10^6$	2.8 ± 0.1	2716.4 ± 64.9	56.1 ± 0.4

decreased with the addition of RWF, as shown in Table III, owing to the decreased deformability of PLA because of the restriction offered by the rigid filler particles.

The modulus of the PLA-RWF composites increased significantly when compared with PLA (Table III). The increment in modulus is almost three- and fourfold with the addition of 10 and 20% RWF, respectively. This can be partially attributed to the much higher modulus exhibited by the RWFs compared with the PLA matrix.[36]

The addition of RWF did not have a significant impact on the tensile strength of the materials, as indicated in Table III; thus, the tensile strength of the filled composites was found to be consistent with the virgin PLA. This shows that good interfacial adhesion was achieved between PLA and RWF, which might be due to the coupling agent silane used in this study. This agrees with findings from the literature[18,19,37–39,40–42] that states the use of a coupling agent can enhance the mechanical properties of filled composites.

Theoretical prediction of Young's modulus

A theoretical model to predict Young's modulus, based on empirical equations developed by Halpin and Tsai[43] (H-T), is presented in this section. For a comparison of theoretical and experimental results, it is assumed that the RWFs are straight and completely randomly oriented in PLA matrix.

The Young's modulus, E_r, of a randomly oriented short fiber composite is given by H-T as:

$$E_r = \frac{3}{8}E_L + \frac{5}{8}E_T \tag{3}$$

where E_L and E_T are longitudinal and transverse moduli, given later:

$$E_L = E_m\left[\frac{1 + (2l/d)\eta_L V_f}{1 - \eta_L V_f}\right] \text{ and } E_T = E_m\left[\frac{1 + 2\eta_T V_f}{1 - \eta_L V_f}\right] \tag{4}$$

The constants η_L and η_T are given as:

$$\eta_L = \frac{(E_f/E_m) - 1}{(E_f/E_m) + (2l/d)} \text{ and } \eta_T = \frac{(E_f/E_m) - 1}{(E_f/E_m) + 2} \tag{5}$$

in eqs. (3)–(5), E_f, E_m, V_f, and l/d are defined as:

E_f, Young's modulus of reinforcement (RWF); E_m, Young's modulus of polymer (PLA); V_f, volume fraction of reinforcement; l/d, aspect ratio of reinforcement.

The RWF used in this study consists of many types of fibers. A microscopic study revealed that RWF consists mainly of aspen, pine, oak, maple, and basswood; thus, RWF is a mixture of both softwood and hardwood. According to the literature,[21] the modulus of softwood varies from 10 to 50 GPa and that of hardwood varies from 10 to 70 GPa. For the theoretical model, three values for the RWF modulus were used, i.e., 30, 40, and 50 GPa, to observe the trend in accordance with the experimental results and to see which value best fit the experimental results.

As shown in the SEM images of RWF (Fig. 1) and PLA-RWF composites (Figs. 3 and 4), the aspect ratio of RWF varies as it is a mixture of various wood fibers. Thus, to simulate the variation, three different aspect ratios of RWF were chosen that differed by a factor of 10, i.e., 10, 100, and 1000. With the three values of the RWF modulus selected along with the three values of aspect ratios of RWF, the modeling was carried out and the results were obtained. Figure 8(a–c) shows the variation of effective elastic modulus of the PLA-RWF composites with RWF content for the three different aspect ratios, i.e., 10, 100, and 1000, respectively. At each aspect ratio, the elastic modulus of the PLA-RWF composite was computed for the three different RWF modulus, i.e., 30, 40, and 50 GPa. As shown in Figure 8(a), for an RWF aspect ratio of 10, the effective elastic modulus of the composite was underestimated (with respect to the experimental results) for all three RWF moduli chosen. When the aspect ratio was increased to 100 [Fig. 8(b)], the effective elastic modulus of the composite increased to values that were close to the experimental results. When the aspect ratio was increased to 1000, the effective elastic modulus further increased to values that were higher than the experimental results when the RWF modulus is 40 or 50 GPa.

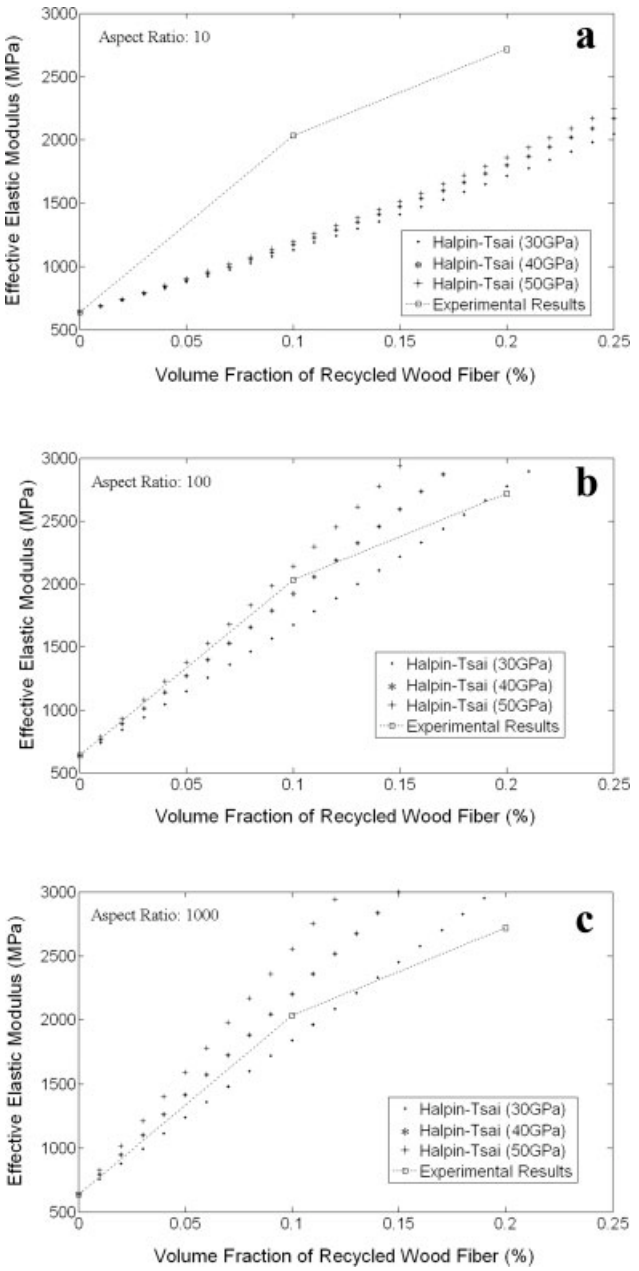

Figure 8 Comparison of Halpin–Tsai[43] and experimental results for Young's modulus of the PLA-RWF composites at various RWF aspect ratios: (a) 10; (b) 100; (c) 1000.

Figure 8(a–c) shows that the effective elastic modulus predicted (1) at an RWF aspect ratio of 100 and RWF modulus of 40 GPa and (2) at an RWF aspect ratio of 1000 and RWF modulus of 30 GPa, coincided closely with the experimental results. However, a perfect fit could not be observed between the theoretically predicted effective composite modulus and that of experimentally measured ones. This might be due to, but not limited to, the following factors[44–46]:

1. The model does not account for the interface between the RWF and PLA.

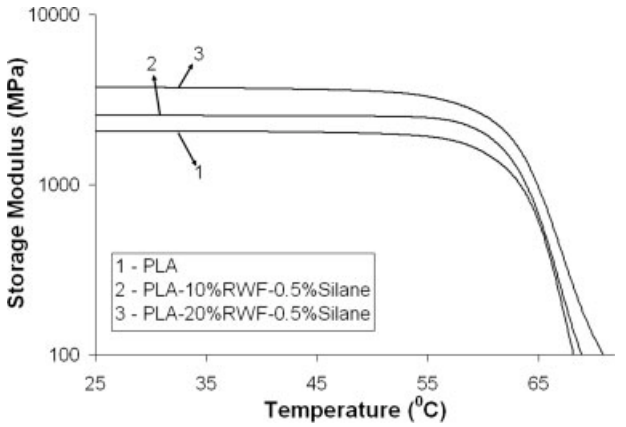

Figure 9 Storage modulus of the PLA-RWF composites as a function of temperature.

2. The model does not account for the waviness in the RWF structure within the PLA matrix.

Thus, it is largely believed that the model can be further developed with the inclusion of the abovementioned factors. Although literature is available in the public domain that accounts for interface and statistical variations in predicting the modulus of fiber composites, a comprehensive study on these aspects is beyond the scope of this article. For a more detailed study, please refer to work done by Fisher et al.[46] and Pilla et al.[47]

Dynamic mechanical properties

The viscoelastic properties of PLA and PLA-RWF composites were investigated using DMA. As shown in Figure 9, the addition of RWF increased the storage modulus with the highest increment for PLA-20%RWF-0.5%Silane specimen. Figure 10 shows the storage modulus at 40°C as a function of the RWF loading level. For example, at 40°C, the storage modulus of PLA is 2046 MPa, while the same for PLA-

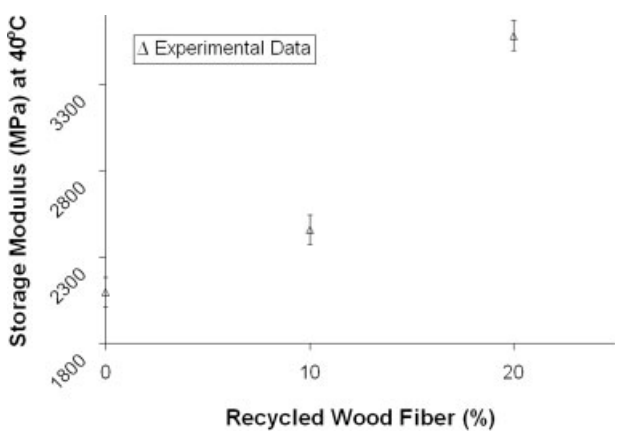

Figure 10 Storage modulus (at 40°C) of the PLA-RWF composites as a function of the RWF content.

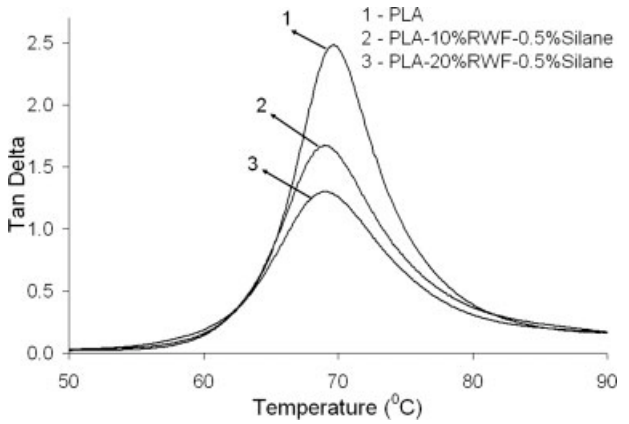

Figure 11 Loss factor (tan δ peak) of the PLA-RWF composites as a function of temperature.

10%RWF-0.5%Silane and PLA-20%RWF-0.5%Silane is 2531 and 3669 MPa, respectively.

The loss factor (tan δ), which is the ratio of loss modulus to storage modulus, is shown in Figure 11. The addition of RWF did not affect the T_g significantly. The values of the T_gs, as computed from the peak of loss modulus, for PLA, PLA-10%RWF-0.5%Silane, and PLA-20%RWF-0.5%Silane were 69.2, 69.1, and 68.9°C, respectively. The area of integration under the tan δ curve decreased with the RWF content, indicating less damping in the PLA-RWF composites. Thus, the PLA-RWF composites exhibited more elastic behavior with increasing RWF, which is in accordance with the tensile test results.

CONCLUSIONS

PLA and PLA-RWF composites with 10 and 20 wt % RWF loading levels were processed using a K-mixer and an injection-molding machine. A M_n analysis on processed PLA and PLA-RWF composites showed that pure PLA and PLA-10%RWF-0.5%Silane composites did not experience degradation during the process, but significant degradation was observed with the PLA-20%RWF-0.5%Silane composite. DSC measurements showed that the addition of RWF reduced the cold crystallization temperature and increased the degree of crystallinity of PLA. The tensile modulus increased with the RWF content, whereas the toughness and strain-at-break decreased. The tensile strength remained the same irrespective of the filler content. A theoretical study on predicting the Young's modulus of the PLA-RWF composites was conducted using the H-T empirical model. Of all the combinations of the modulus and aspect ratio of RWF studied, it was found that an aspect ratio of 100 and RWF modulus of 40 GPa and an aspect ratio of 1000 and RWF modulus of 30 GPa coincide closely with experimental results. The storage modulus increased and the area under the tan δ curve decreased with the RWF content.

The authors acknowledge Gray Slough and David Jacobson of TA instruments for providing insight on polymer aging. They also acknowledge James Muehl and Alex Wiedenhoeft of the USDA Forest Products Laboratory for providing information on various types of fibers present in the recycled wood fiber mixture.

References

1. Gross, R. A.; Kalra, B. Science 2002, 297, 803.
2. Bastioli, C. Starch/Staerke 2001, 53, 351.
3. Pilla, S.; Gong, S.; O'Neill, E.; Rowell, R. M.; Krzysik, A. M. Polym Eng Sci 2008, 48, 578.
4. Drumright, R. E.; Gruber, P. R.; Henton, D. E. Adv Mater 2000, 12, 1841.
5. Fang, Q.; Hanna, M. A. Ind Crop Prod 1999, 10, 47.
6. Anderson, K.; Lim, S. H.; Hillmyer, M. A. J Appl Polym Sci 2003, 89, 3757.
7. Hiljanen-Vainio, M.; Kylma, J.; Hiltunen, K; Seppala, J. V. J Appl Polym Sci 1997, 63, 1335.
8. Huda, M. S.; Drzal, L. T.; Misra, M.; Mohanty, A. K. Ind Eng Chem Res 2005, 44, 5593.
9. Huneault, M. A.; Li, H. Polymer 2007, 48, 270.
10. Eckert, C. Proceedings of Progress in Woodfibre-Plast Composites, Toronto, ON, 2000.
11. Mohanty, A. K.; Misra, M.; Drazel, L. T. J Polym Environ 2002, 10, 19.
12. Samir, M. A. S. A.; Allioin, F.; Dufresne, A. Biomacromolecules 2005, 6, 612.
13. Bledzki, A. K.; Gassan, J. Prog Polym Sci 1999, 24, 221.
14. Clemons, C. Forest Prod J 2002, 52, 10.
15. Wegner, T. H.; Youngquist, J. A.; Rowell, R. M. Proc Mater Res Soc Symp 1992, 266, 3.
16. Mohanty, A. K.; Misra, M.; Hinrichsen, G. Macromol Mater Eng 2000, 276/277, 1.
17. Yu, L.; Petinakis, S.; Dean, K.; Bilyk, A.; Wu, D. Macromol Symp 2007, 249/250, 535.
18. Xue, Y.; Veazie, D. R.; Glinsey, C.; Horstemeyer, M. F.; Rowell, R. M. Composites B 2007, 38, 152.
19. Colom, X.; Carrasco, F.; Pages, P.; Canavate, J. Comp Sci Technol 2003, 63, 161.
20. Rezgui, F.; Swistek, M.; Hiver, J. M.; G'Sell, C.; Sadoun, T. Polymer 2005, 46, 7370.
21. Lilholt, H.; Lawther, J. M. In Comprehensive Composite Materials, Vol. 1: Fiber Reinforcements and General Theory of Composites; Chou, T. W., Ed.; Elsevier: New York, 2000; Chapter 1.10, p 303.
22. Agarwal, B.; Broutman, L. Analysis and Performance of Fiber Composites; Wiley: New Jersey, 1990.
23. Mathew, A. P.; Oksman, K.; Sain, M. J Appl Polym Sci 2005, 97, 2014.
24. Zheng, X.; Li, J.; Zhou, Y. Acta Mater 2004, 52, 3313.
25. Garlotta, D. J Polym Environ 2002, 9, 63.
26. Nam, P. H.; Maiti, P.; Okamoto, M.; Kotaka, T.; Nakayama, T.; Takada, M.; Ohshima, M.; Usuki, A.; Hasegawa, N.; Okamoto, H. Polym Eng Sci 2002, 42, 1907.
27. Hodge, I. M. Macromolecules 1983, 16, 898.
28. Hodge, I. M.; Huvard, G. S. Macromolecules 1983, 16, 361.
29. Behrens, A. R.; Hodge, I. M. Macromolecules 1982, 15, 756.
30. Turi, E. A., Ed. Thermal Characterization of Polymeric Materials, 2nd ed.; Academic Press, 1997; Vol. 1, p 556.
31. Masirek, R.; Kulinski, Z.; Chionna, D.; Piorkowska, E.; Pracella, M. J Appl Polym Sci 2007, 105, 255.

32. Pracella, M.; Chionna, D.; Anguillesi, I.; Kulinski, Z.; Piorkowska, E. Compos Sci Technol 2006, 66, 2218.
33. Wu, D.; Wu, L.; Wu, L.; Xu, B.; Zhang, Y.; Zhang, M. J Polym Sci Part B: Polym Phys 2007, 45, 1100.
34. Van Vlack, L. H. Elements of Materials Science and Engineering, 6th ed.; Addison-Wesley Publishing: Massachusetts, USA, 1989; p 271.
35. Kompella, M. K.; Lambros, J. Polym Test 2002, 21, 523.
36. Nunez, A. J.; Sturm, P. C.; Kenny, J. M.; Aranguren, M. I.; Marcovich, N. E.; Reboredo, M. M. J Appl Polym Sci 2003, 88, 1420.
37. Liao, B.; Huang, Y.; Cong, G. J Appl Polym Sci 1997, 66, 1561.
38. Kokta, B. V.; Deneault, C. Polym Compos 1986, 7, 337.
39. Raj, R. G.; Kokta, B. V.; Maldas, D.; Deneault, C. Polym Compos 1988, 9, 404.
40. Maldas, D.; Kokta, B. V. J Adhes Sci Technol 1991, 5, 727.
41. Maldas, D.; Kokta, B. V.; Raj, R. G.; Sean, S. T. Mater Sci Eng A 1988, 104, 235.
42. Simonsen, J.; Jacobsen, R.; Rowell, R. J Appl Polym Sci 1998, 68, 1567.
43. Halpin, J. C.; Tsai, S. W. US Airforce Technical Report; AFML TR, 67–423, 1967.
44. Shi, D. L.; Feng, X. Q.; Huang, Y.; Hwang, K. C.; Gao, H. J Eng Mater Technol 2004, 126, 250.
45. Shi, D. L.; Feng, X. Q.; Huang, Y.; Hwang, K. C. Key Eng Mater 2004, 261–263, 1487.
46. Fisher, F. T.; Bradshaw, R. D.; Brinson, L. C. Compos Sci Technol 2003, 63, 1689.
47. Pilla, S., Hammitt, A., Nikolaidis, E. J Mater Manuf SAE Trans 2006, 115, 111.